



On the application of photocatalyst-sorbent composite materials for arsenic (III) remediation: Insights from kinetic adsorption modelling

Jay C. Bullen^{a,*}, Chaipat Lapinee^{b,c}, Pascal Salaün^d, Ramon Vilar^c, Dominik J. Weiss^{a,e,*}



^a Department of Earth Science and Engineering, Imperial College London, London SW7 2AZ, United Kingdom

^b Department of Chemistry, School of Science, University of Phayao, Phayao 56000, Thailand

^c Department of Chemistry, Imperial College London, White City Campus, London W12 0BZ, United Kingdom

^d School of Environmental Sciences, University of Liverpool, Liverpool L69 3GP, United Kingdom

^e Civil and Environmental Engineering, Princeton University, United States of America

ARTICLE INFO

Editor: G.L. Dotto

Keywords:

Batch
Continuous flow
Arsenic remediation
Remediation
Pseudo-Second order
Adsorption kinetics

ABSTRACT

TiO₂-Fe₂O₃ composites show great promise for the removal of arsenic(III) from drinking water: this single material combines the photocatalytic capabilities of TiO₂ for the oxidation of arsenite (i.e. As(III)) with the high adsorption capacity of iron oxides towards the arsenate (i.e. As(V)) subsequently produced. To design an effective treatment, it is necessary to balance high sorbent concentrations, providing long filter lifetimes, with low photocatalyst concentrations, to achieve effective penetration of light into the system. In this work, we construct a predictive model using experimentally determined As(III) adsorption isotherms and kinetics to estimate arsenic treatment plant lifetimes. We considered sorbent loading, treatment time, and batch treatment versus continuous-flow. Our model indicated that batch treatment is more efficient than continuous-flow at low sorbent concentrations (< 100 g L⁻¹), and therefore more appropriate for the photocatalyst-sorbent system. However, with < 100 g L⁻¹ sorbent, media should be replaced several times per year to maintain effective treatment. In contrast, slurries of > 100 g L⁻¹ sorbent could operate for an entire year without media replacement. This work highlights the important implications of sorbent concentration when we consider the multifunctional photocatalysts-sorbent system, and highlights the need for further experimental work to design efficient arsenic treatment plants.

1. Introduction

The arsenic treatment plants developed for South Asia often fail to provide safe drinking water [1]. One study of 200 plants in rural Uttar Pradesh, India, found that after 10 years only 34 plants were still in operation, of which only one was delivering water below the 10 µg L⁻¹ WHO safety limit [1]: the remaining 97% of treatment plants were providing unsafe water. Much of the difficulty in providing safe water in South Asia lies in the anoxic, reducing groundwater conditions, where arsenic is found in the +3 oxidation state, i.e. neutral H₃AsO₃, which adsorbs weakly to sorbent media. Pre-oxidation of arsenite, As(III), to more strongly adsorbing, negatively charged arsenate, As(V), oxyanions (i.e. H₂AsO₄⁻ and HAsO₄²⁻ at neutral pH) is thus important for effective removal [2]. Whilst oxidation of As(III) can be achieved through application of conventional chemical oxidants such as chlorine, permanganate, ozone, and Fenton's reagent [3,4], limitations include the risk of toxic disinfection by-products (DBPs) such as carcinogenic

trihalomethanes (particularly relevant in South Asia due to the high levels of dissolved organic matter present in arsenic-contaminated groundwaters) [4,5]. Oxidation using heterogeneous photocatalysts such as TiO₂ reduces the risk of DBPs [6], and mixed mineral oxide composites such as TiO₂-Fe₂O₃ are especially attractive, as they combine photocatalytic oxidation of As(III) to As(V), using the TiO₂ phase, with effective adsorption of As(V) to the Fe₂O₃ phase [7–9].

To date, however, photocatalyst-sorbent materials remain untested for real-life applications in As(III) remediation. An important yet unanswered question when engineering the photocatalyst-sorbent system is how much material should be used. Low concentrations of suspended photocatalysts (< 1 g L⁻¹) are typical for As(III) photooxidation, to achieve effective light penetration through the system [10–14]. Whilst linear relationships between TiO₂ concentrations and reaction rates are often observed at low catalyst concentrations, at high catalyst concentrations reaction rates become limited by the supply of photons and by light scattering effects [12]. Reaction rates may even decrease with

* Corresponding authors.

E-mail addresses: j.bullen16@imperial.ac.uk (J.C. Bullen), d.weiss@imperial.ac.uk (D.J. Weiss).

excess photocatalyst concentrations [15]. However, low sorbent concentrations lead to low adsorption capacities and limited filter lifetimes, after which saturated sorbent media (i.e. with no adsorption capacity remaining) must be replaced or regenerated. Sorbent life-time is a major factor determining the success or failure of arsenic mitigation schemes in South Asia: users often fail to replace or regenerate saturated sorbent media due to lack of expertise [16] or lack of confidence [17]. A recent study of three arsenic mitigation microenterprises across India and Bangladesh found that the robustness and reliability of the sorbent material was the most important technological factor for sustaining and growing these schemes [18].

Another challenge to sustaining arsenic remediation programs is the cost of replacement sorbent media [16]. Improving economic efficiency requires maximising the concentration of arsenic loaded on the sorbent before breakthrough (breakthrough is where the material is saturated, and arsenic emerges in the effluent). Factors affecting sorbent economy include not just the amount of sorbent used, but also how it is used, e.g. the choice between batch and continuous-flow treatments [19]. In a batch treatment, discrete volumes of water are treated sequentially, for a designated time, after which the effluent hopefully meets safety guidelines. In a continuous-flow treatment, influent and effluent are continuously pumped into and out of the reactor, and flow-rate becomes another consideration. Sorbent economy is improved with slow flow rates, but users of household arsenic filtration systems have previously complained that the flow-rates of current products are too slow [17].

The efficiency of different treatment designs can be defined both by their sorbent economy and the volume of water treated before the effluent exceeds the maximum contaminant level (MCL). Most household and community-scale solutions for the treatment of arsenic-contaminated water use sorbent media in a continuous-flow, column arrangement [1,20]. It is commonly believed that continuous-flow adsorption is more efficient than batch treatment, but under certain conditions batch treatment can prove superior [19], and despite many studies on novel sorbents conducting both batch and column experiments, few papers provide a comparison between the merits of each treatment. In the field of environmental remediation, photocatalysts are also deployed in both batch and continuous-flow devices [21]. Photocatalytic performance can vary between the two processes, e.g. one study found that photocatalytic degradation of dyes was up to 110% more effective under continuous-flow treatment [15]. It is non-trivial to compare the efficiency of batch and continuous-flow treatments, for instance batch treatments are defined by the time required (minutes per unit volume) whilst continuous-flow is defined by the rate (volume per minute) and bed volumes treated before breakthrough, and subsequently the lack of substantive cross-evaluation is not surprising [22].

Previous work on relative merits of batch and continuous-flow design includes the study of Dichiara et al., where a 'critical concentration' parameter was calculated from experimentally determined coefficients (pertaining to the fixed bed sorbate removal efficiency, and incorporating effects such as pore channelling) [19]. When the target effluent concentration (e.g. the MCL) exceeds this critical concentration, batch treatment gives a better sorbent economy than fixed bed column treatments, and vice versa. Lekić et al. compared the efficiencies of their sorbent (iron-manganese oxide coated sand) for As(III) and As(V) removal in batch and column configurations by comparing the amount of arsenic removed per gram of sorbent [23]. They found that continuous-flow columns were more efficient than batch treatment, which they suggested was due to non-adsorption processes such as coagulation, flocculation and filtration [23].

The risk of exposure to arsenic contaminated water in South Asia is greatest amongst the rural poor [24,25]. Rural communities often lack access to replacement parts and expertise in maintaining filter systems, two major reasons for the short-lifetimes of arsenic mitigation schemes [16]. Electrical outages [26] and the challenge of maintaining equipment [17] mean that a system based on multifunctional photocatalytic

sorbents needs a fail-safe option, i.e. the device should provide reasonable removal of As(III) in the absence of photooxidation.

The aim of this work was to determine the minimum concentration of $\text{TiO}_2\text{-Fe}_2\text{O}_3$ needed for an arsenic treatment plant, considering the worst-case scenario that the material is operated as a sorbent only. To achieve this aim, our objectives were: (1) to experimentally determine adsorption isotherms and kinetics as input parameters for simulating the As(III)/ $\text{TiO}_2\text{-Fe}_2\text{O}_3$ system; (2) to develop a kinetic model capable of describing As(III) adsorption that is sensitive to changes in both sorbent and sorbate concentration; (3) to investigate the influence of sorbent concentration on batch and continuous-flow treatments; (4) to investigate sorbent life-times in both systems, simulating a single household's clean water requirement over a 365-day period; and finally (5) to recommend a reactor design for use in subsequent experimental work.

2. Experimental

2.1. Synthesis of a $\text{TiO}_2\text{-Fe}_2\text{O}_3$ bi-functional sorbent

The synthesis of a $\text{TiO}_2\text{-Fe}_2\text{O}_3$ bi-functional sorbent was carried out in two steps, by small modifications of a previously reported procedure [27,7]. Firstly, mesoporous anatase TiO_2 was produced via sol-gel synthesis [28]. For this, pluronic P123 (1 g, Aldrich) was dissolved in absolute ethanol (12 g, VWR, ACS Puriss grade), and $\text{Ti(OBu}^n\text{)}_4$ (2.7 g, ACROS Organics, 99% purity) was dissolved in concentrated HCl (3.2 g, ACROS Organics, ACS reagent grade, ca. 37%). The P123 solution was added dropwise to the solution of $\text{Ti(OBu}^n\text{)}_4$ and the mixture was aged at room temperature with continuous stirring, until a gel-like white film of TiO_2 was formed. The product was calcined at 350 °C for 4 h (temperature ramped at 1 °C min⁻¹), cooled to room temperature, and then crushed. In the second step, this mesoporous TiO_2 (1.5 g) was added to an ethanolic solution of 0.6 M $\text{Fe(NO}_3)_3\text{·9H}_2\text{O}$ (48.5 g, Sigma-Aldrich, ACS reagent grade, > 98%). The mixture was stirred for 30 min, then heated at 50 °C to evaporate the solvent. The product was calcined in a furnace at 300 °C for 10 min, then cooled and crushed. The product was calcined a final time, at 300 °C for 6 h. The material was ground to a homogeneous powder and stored in a desiccator. The theoretical $\text{TiO}_2\text{-Fe}_2\text{O}_3$ mass ratio was 1:1, based on the quantities of reagents used. $\text{TiO}_2\text{-Fe}_2\text{O}_3$ was characterised using XRD and SEM, and the BET-specific surface area, surface charge, and zeta potential were determined, as discussed in the Supplementary Information.

2.2. Determination of adsorption capacity and kinetic parameters

Adsorption isotherms and kinetic parameters for the arsenic treatment plant model were obtained, with the experimental procedure described in the Supplementary Information. Briefly, adsorption isotherms were determined and then modelled using the Langmuir and Freundlich equations [29]. Adsorption kinetics were determined and then modelled using the pseudo-first and pseudo-second order rate equations [30]. As(III) concentrations were determined electrochemically by Anodic Stripping Voltammetry (ASV) [31–33]. Experiments were carried out in triplicate and uncertainties were calculated as the standard deviation between results. For adsorption isotherm parameters, uncertainties were propagated from the standard error in the slope and y-intercept of the linearised plots. For pseudo-second order kinetic parameters, uncertainties were determined using the Monte Carlo nonlinear regression method reported by Hu et al. [34].

2.3. Predictive modelling of adsorption kinetics

The kinetic adsorption model aimed to investigate As(III) removal under different initial sorbate (C_0) and sorbent (C_s) concentrations. A demonstration of how the pseudo-second order (PSO) model can be modified to provide better sensitivity towards changes in C_0 and C_s is

given elsewhere [35], with a modified rate equation that takes the form:

$$\frac{dq}{dt} = k' C_t \left(1 - \frac{q_e}{q_t}\right)^2 \quad (1)$$

where dq/dt is the rate of change in the concentration of adsorbed As(III) ($\text{mg g}^{-1} \text{ min}^{-1}$), t is time (min), q_t and q_e are the concentrations of As(III) adsorbed at time t and at equilibrium, respectively (mg g^{-1}), k' is the rate constant ($\text{L g}^{-1} \text{ min}^{-1}$), C_t is the concentration of aqueous As(III) at time t (mg L^{-1}), and k' is derived from PSO parameters via:

$$k' = \frac{k_2 q_e^{\dagger 2}}{C_0^{\dagger}} \quad (2)$$

where k_2 is the PSO rate constant ($\text{g mg}^{-1} \text{ min}^{-1}$), and q_e^{\dagger} (mg g^{-1}) and C_0^{\dagger} (mg L^{-1}) denote the values of q_e and C_0 under the original experimental conditions [35]. The expression for second-order dependence upon the relative amount of available adsorption capacity remaining, $\left(1 - \frac{q_e}{q_t}\right)^2$, is the same expression seen elsewhere, such as in the integrated kinetic Langmuir model [36]. In this modified kinetic model, q_e was calculated at each point in time using the experimentally determined Freundlich adsorption isotherm, given by:

$$q_e = K_F C_e^{1/n} \quad (3)$$

where C_e is the concentration of aqueous sorbate at equilibrium (mg L^{-1}), and the Freundlich constant, K_F ($\text{mg g}^{-1} (\text{mg L}^{-1})^{-1/n}$) and n (unitless) are experimentally determined constants [29]. It has been shown that using adsorption isotherms to calculate the PSO parameter q_e outside of equilibrium, at each point in time, gives a better account of initial adsorption kinetics than when using the fixed value of q_e calculated from the linearised PSO kinetics [37].

2.4. Continuous-flow model

The continuous flow reactor design was modelled by adding terms to Eq. (1) that account for influx and outflux of As(III) with continuous pumping:

$$\frac{dC}{dt} = jC_{\text{influent}} - C_s k' C_t \left(1 - \frac{q_e}{q_t}\right)^2 - jC_t \quad (4)$$

where dC/dt is the rate of change in the concentration of As(III) ($\text{mg L}^{-1} \text{ min}^{-1}$), j is the reactor turnover rate (min^{-1}), indicating the time taken to produce one bed volume of effluent, and C_{influent} is the concentration of influent As(III) (mg L^{-1}). jC_{influent} reflects the increase in C_t due to influx of the influent, whilst jC_t represents As(III) lost via the effluent.

Continuous flow reactors were modelled with C_s varied between 0.01 and 10 000 g L^{-1} and C_0 was set at 0.5, 1, or 2 mg L^{-1} . The parameter j was varied between 0.001 and 1 min^{-1} to reflect reactor residence times (i.e. treatment times) between one minute and one day.

2.5. Modelling 365 days of treatment

To model 365 days of sequential batch treatments using the same mass of sorbent, we considered a reactor operated once per day on a single volume of water, as per Colombo and Ashokkumar [15]. 365 consecutive simulations were conducted, each representing a single day: in each simulation the initial value of q_t was set equal to the final value of q_t in the previous simulation, to reflect increasing saturation of the sorbent with each passing day. The size of the reactor was set as 40 L per household to meet clean water requirements, and the quantity of sorbent needed was calculated using mass of sorbent (g household^{-1}) = V (40 L household^{-1}) $\cdot C_s$ (g L^{-1}).

To model the continuous-flow system, (a) the number of bed volumes successfully treated in 365 days

(BV (year^{-1}) = j (min^{-1}) $\cdot 525\,600$ (min year^{-1})) and (b) the number of bed volumes treated before breakthrough were both determined, and the lesser of the two was used as a measure of the volume of safe water produced in 365 days. The size of the reactor was calculated as the minimum size required to provide 40 L $\text{household}^{-1} \text{ day}^{-1}$, using equation V (L) = 40 ($\text{L household}^{-1} \text{ day}^{-1}$) $\cdot j$ (min^{-1}) $\cdot 1440$ (min day^{-1}). In both systems, sorbent efficiency was determined as the concentration of As(III) either (a) adsorbed at breakthrough, or (b) after 365 days (whichever came sooner). The ‘average residence time’ (min) was calculated as the inverse of turnover rate.

2.6. Simulations using MATLAB

Differential equations (Eqs. (1) and (4)) were solved using custom-built MATLAB codes, provided in the Supplementary Information [38].

For each simulation, the input parameters were C_0 , C_s , C_{influent} , j , k' , K_F , n and q_0 (where q_0 is the initial concentration of adsorbed As(III), being only non-zero when simulating 365 days of batch treatment). The end-point of each simulation was set as 1440 min for the batch system, and calculated as a product of C_{influent} and j^{-1} for the continuous-flow system. 2000 data points were calculated, with shorter time intervals during the initial stages of reaction (where C_t and q_t are fastest to change), giving better resolution. The differential equations were solved using the ODE15s and ODE45 functions and the output was saved to a .txt file.

For both systems As(III) concentrations of 500 and 2000 $\mu\text{g L}^{-1}$ were considered, representing the most severe arsenic contamination observed in South Asia [39]. The system was simplified by not including phosphate and sulphate anions which would compete with arsenic for sorbent binding sites. K_F was rescaled to better fit the kinetic data, owing to an increase in the adsorption of As(III) at $C_e = 23 \text{ mg L}^{-1}$ observed in the kinetic experiment compared with the adsorption isotherm.

3. Results and discussion

3.1. Determining parameters for modelling adsorption capacity

Understanding adsorption capacity and adsorption mechanisms is essential for developing kinetic adsorption models. As(III) adsorption isotherms at pH 5, 7 and 9 were determined and modelled using the Langmuir and Freundlich adsorption isotherms (Fig. 1). Isotherm parameters are presented in Table 1. On average, the Freundlich adsorption isotherm model gave a better fit ($R^2 = 0.7996 \pm 0.0786$) than the Langmuir model ($R^2 = 0.7583 \pm 0.0347$), however results were within error of one another.

Previous studies have also fit As(III) adsorption onto TiO_2 and Fe_2O_3 using both isotherm models. Examples of Freundlich behaviour at circumneutral pH include Gupta et al. (TiO_2) [40] and Tang et al. (Fe_2O_3) [41]. Examples of Langmuir-type behaviour at circumneutral pH include Pan and Hu (TiO_2) [42] and Giménez (Fe_2O_3) [43]. Dutta et al. found a superior fit with the Freundlich adsorption isotherm for As(III) adsorption onto TiO_2 at pH 4 and 9 [44]. Deedar et al. found that As(III) adsorption onto TiO_2 was best described by the Langmuir adsorption isotherm, however, it is unclear whether the difference was statistically significant [45]. In this work, As(III) adsorption capacities were higher than the previously reported capacities for As(V) adsorption onto $\text{TiO}_2\text{-Fe}_2\text{O}_3$ with 12.14 ± 0.42 , 7.79 ± 0.20 and $6.48 \pm 0.30 \text{ mg g}^{-1}$, at pH 5, 7 and 9, respectively [27]. This is potentially due to multilayer adsorption of As(III), which has been identified in several studies [46]. The Freundlich adsorption model was subsequently used throughout the rest of this work.

Maximum adsorption of As(III) occurred at pH 5 (Fig. 1). Previous studies of composite photocatalyst-sorbents include $\gamma\text{-Fe}_2\text{O}_3@\text{ZrO}_2$, which showed maximum As(III) adsorption at pH 8–9 [47], and iron-doped TiO_2 , with a maximum at pH 7 [45]. As(III) adsorption onto TiO_2

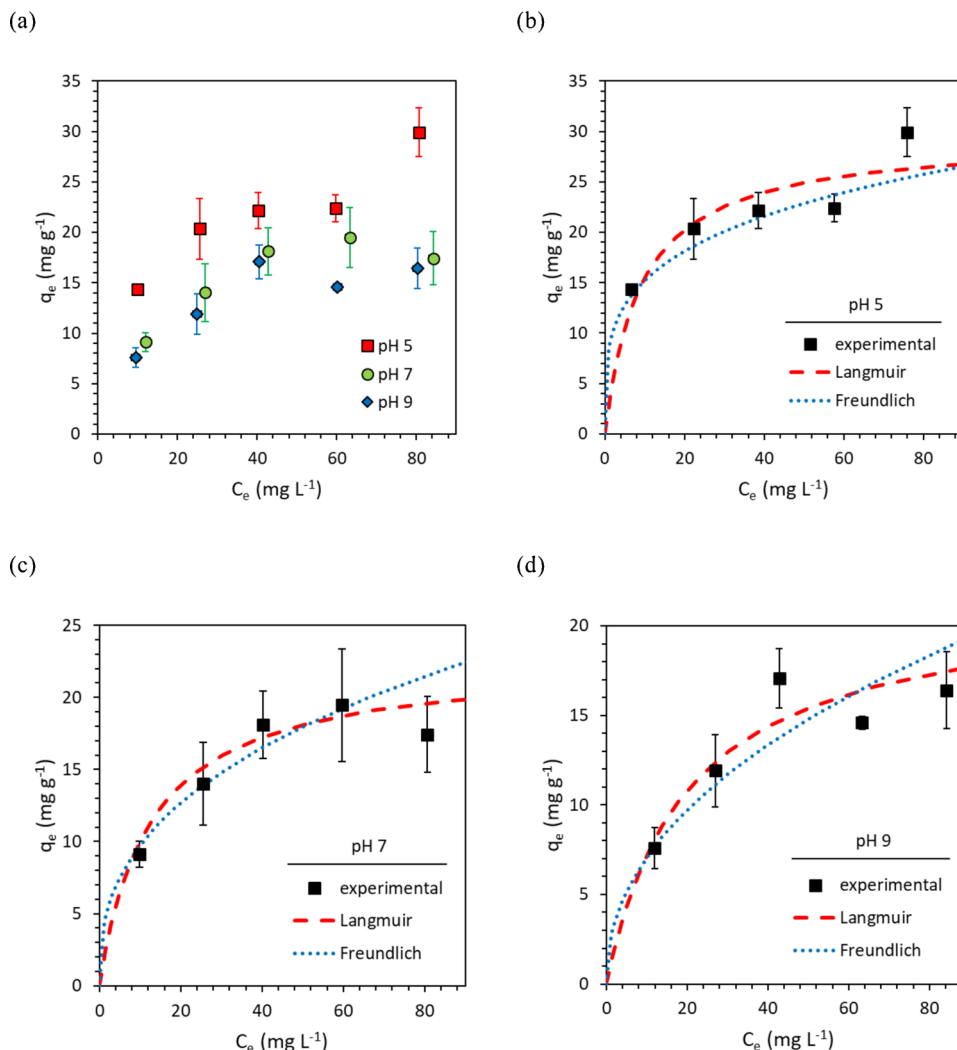


Fig. 1. As(III) adsorption isotherms using the $\text{TiO}_2\text{-Fe}_2\text{O}_3$ multifunctional sorbent. The influence of pH on adsorption isotherms is presented in (a), and a comparison of Langmuir and Freundlich adsorption isotherms is made at (b) pH 5, (c) pH 7, and (d) pH 9. Experimental conditions were 20–100 mg L⁻¹ total As(III), 1 g L⁻¹ sorbent, and buffered electrolytes: either 0.01 M acetate (pH 5), 0.01 M HEPES (pH 7), or 0.01 M borate (pH 9). Error bars show the standard deviation between three repeat experiments.

typically shows a maximum at alkaline pH values: at pH 8 [42], pH 9 [40] or pH 8–10 [48], whilst As(III) demonstrates maximum adsorption onto iron oxides at lower pH, for instance pH 6 for Fe_2O_3 [49]. The $\gamma\text{-Fe}_2\text{O}_3$ nanosheets reported by Liu et al. showed increasing As(III) adsorption with increasing acidity, down to pH 3 [50]. The increased adsorption of As(III) at pH 5 suggests that adsorption to our $\text{TiO}_2\text{-Fe}_2\text{O}_3$ composite is primarily controlled by the Fe_2O_3 phase, rather than by TiO_2 .

Table 1

Langmuir and Freundlich parameters for As(III) adsorption onto $\text{TiO}_2\text{-Fe}_2\text{O}_3$. R^2 is the coefficient of determination, representing the goodness of fit between experiment and model in the non-linear adsorption isotherm. For the linear equations, R^2 values were 0.93, 0.97 and 0.94 for Langmuir adsorption isotherms at pH 5, 7 and 9, respectively, and 0.78, 0.88 and 0.84 for Freundlich adsorption isotherms at pH 5, 7 and 9 respectively. Uncertainties were propagated using the standard deviation of the slope and y-intercept parameters of the linear regression. The BET-specific surface area of $\text{TiO}_2\text{-Fe}_2\text{O}_3$ was 63.1 m² g⁻¹.

pH	Langmuir parameters				R^2	Freundlich parameters			
	Q _{max}			K_L		K_F	n	R^2	
	(mg g ⁻¹)	(mg m ⁻²)	(μmol m ⁻²)						
5	29.44 ± 2.99	0.47 ± 0.05	6.21 ± 0.66	0.11 ± 0.07	0.7219	8.47 ± 2.64	3.94 ± 0.95	0.8835	
7	22.64 ± 1.74	0.36 ± 0.03	4.81 ± 0.37	0.08 ± 0.03	0.7909	4.06 ± 1.15	2.63 ± 0.14	0.7874	
9	21.60 ± 0.33	0.35 ± 0.01	4.61 ± 0.09	0.05 ± 0.01	0.7622	2.46 ± 0.75	2.18 ± 0.25	0.7278	

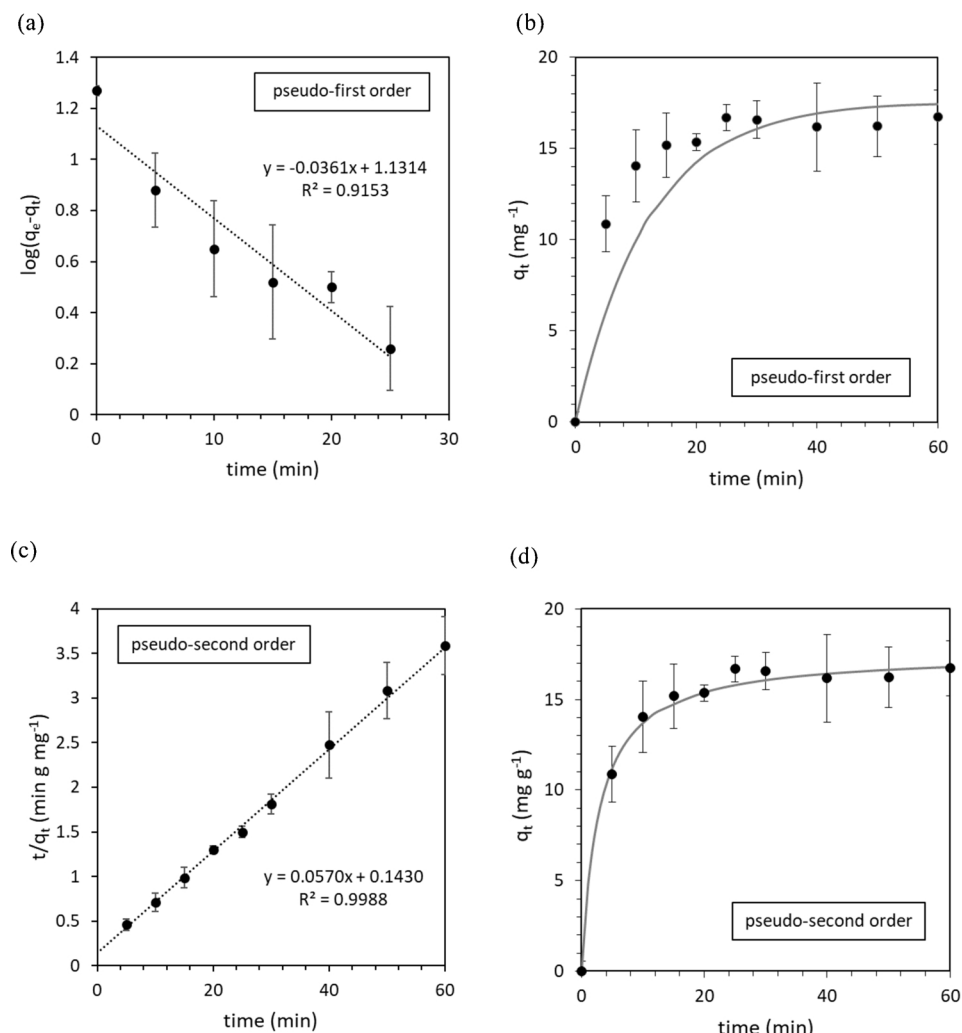


Fig. 2. Kinetics of As(III) adsorption onto $\text{TiO}_2\text{-Fe}_2\text{O}_3$. Experimental conditions were pH 7 (0.01 M HEPES), with 39 mg L^{-1} initial As(III), and 1 g L^{-1} sorbent. The plots show both (a and b) pseudo-first order, and (c and d) pseudo-second order kinetic models, fitted to the experimental data. Error bars indicate the standard deviation between three repeat experiments.

As(III) concentrations decreased very fast within the first 5 min of mixing and reached equilibrium within approximately 25 min (Fig. 2). Slower As(III) adsorption kinetics have been observed for other composite photocatalyst-sorbents, with equilibrium reached in 180 min for $\gamma\text{-Fe}_2\text{O}_3\text{-TiO}_2$ ($C_0 = 1 \text{ mg L}^{-1}$, $C_s = 0.5 \text{ g L}^{-1}$, pH 7.0) [8] and 120 min for $\gamma\text{-Fe}_2\text{O}_3@\text{ZrO}_2$ ($C_0 = 100 \text{ mg L}^{-1}$, $C_s = 1 \text{ g L}^{-1}$, pH 9) [47]. However, Li et al. found that Pb(II) adsorption onto $\text{Fe}_2\text{O}_3\text{-TiO}_2$ composite materials reached equilibrium very rapidly, in just 5 min ($C_0 = 10\text{-}80 \text{ mg L}^{-1}$, $C_s = 1 \text{ g L}^{-1}$) [51].

The experimentally determined kinetic parameters are presented in

Table 2

Experimentally determined kinetic parameters for the adsorption of As(III) onto $\text{TiO}_2\text{-Fe}_2\text{O}_3$. When kinetic data was linearised, R^2 values were 0.9153 for pseudo-first order kinetics and 0.9988 for pseudo-second order kinetics. Experimental conditions were 39 mg L^{-1} initial As(III), 1 g L^{-1} sorbent, and pH 7 (0.01 M HEPES). Pseudo-first order parameters were fit using the first six data points, pseudo-second order parameters were fit using nine data points.

	Pseudo-first order	Pseudo-second order
Rate constant	$k_1 = 0.083 \pm 0.019 \text{ min}^{-1}$	$k_2 = 0.020 \pm 0.002 \text{ g mg}^{-1} \text{ min}^{-1}$
$q_e (\text{mg g}^{-1})$	17.6 ± 0.6	17.6 ± 0.3
R^2	0.7770	0.9928

Table 2. The PFO kinetic model gave a poor fit ($R^2 = 0.7770$), significantly underestimating the rate of adsorption in the first 20 min (Fig. 2a and b). The PSO model, in contrast, provided a very accurate fit to experimental data ($R^2 = 0.9928$, Fig. 2c and d). The PSO rate constant, k_2 , was $0.020 \pm 0.002 \text{ g mg}^{-1} \text{ min}^{-1}$. This lies within the range of literature values for As(III) adsorption to similar multifunctional composite sorbents: $0.12 \text{ g mg}^{-1} \text{ min}^{-1}$ for $\gamma\text{-Fe}_2\text{O}_3\text{-TiO}_2$ [8] and $0.001 \text{ g mg}^{-1} \text{ min}^{-1}$ for $\gamma\text{-Fe}_2\text{O}_3@\text{ZrO}_2$ [47].

3.3. Using a modified pseudo-second order (PSO) model for predictive modelling

We recently demonstrated that the pseudo-second order adsorption model can be modified to provide better sensitivity towards changes in C_0 and C_s [35]. The modified rate equation (Eq. (1)) uses a rate constant, k' , that is readily calculated from experimental PSO parameters via Eq. (2) [35]. Whilst the original PSO model provides no sensitivity towards C_0 and C_s , our modified model gives the first order dependence towards sorbate concentration, C_b , that is typically seen experimentally [35]. This model also incorporates sensitivity to C_s through the adsorption isotherms used to determine q_e [35]. In this work, the Freundlich adsorption isotherm was used to calculate q_e , due to the possibility of multilayer As(III) adsorption [46]. The modified kinetic model was validated through successful reconstruction of the original PSO model's

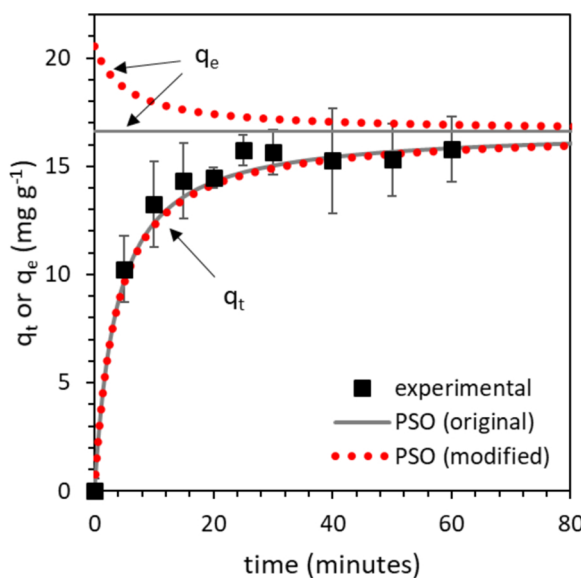


Fig. 3. Comparison of the original PSO model with the modified kinetic adsorption model. The labels ‘ q_t ’ and ‘ q_e ’ indicate the quantity of adsorbed As(III) and the fixed or calculated value of q_e at each time point respectively. Note that the magnitude of the Freundlich constant, K_F , has increased from 4.06 to 5.10 to account for the difference in q_e observed between the adsorption isotherm and kinetic experiments when $C_e = 22.4 \text{ mg L}^{-1}$ (in the Freundlich adsorption isotherm when $C_e = 22.4 \text{ mg L}^{-1}$, $q_e = 13.3 \text{ mg g}^{-1}$, and in the kinetic experiments when $C_e = 22.4 \text{ mg L}^{-1}$, $q_e = 16.7 \text{ mg g}^{-1}$). The models presented are labelled as follows: PSO (original): $\frac{dq}{dt} = k_2(q_e - q_t)^2$, PSO (modified): $\frac{dq}{dt} = k' C_t \left(1 - \frac{q_t}{q_e}\right)^2$ where $k' = \frac{k_2 q_e^{1/n}}{C_0^{1/n}}$ and q_e is calculated at each point in time using the Freundlich adsorption isotherm.

fit to the experimental data (Fig. 3).

3.4. Modelling the performance of an arsenic treatment plant: batch vs continuous-flow design

Input parameters for the kinetic adsorption model were determined experimentally at pH 7 using adsorption isotherms with $C_e = 10 - 80 \text{ mg L}^{-1}$ and $C_s = 1 \text{ g L}^{-1}$, and adsorption kinetics with $C_0 = 39 \text{ mg L}^{-1}$ and $C_s = 1 \text{ g L}^{-1}$. The modelling parameters are presented in Table 3. The neutral pH used is representative of typical groundwaters in South Asia and matches the point of zero charge for TiO₂-Fe₂O₃ (pH 7.0 ± 0.2, Supplementary Information), and is thus appropriate for modelling small scale treatment systems where pH is not optimised. A relatively high value of C_0 used in the experimental work was chosen to increase accuracy and precision in the reported data, however it is over an order of magnitude greater than the C_0 values being modelled. The experimental sorbent loading, C_s (1 g L⁻¹) is at the upper end of typical photocatalyst concentrations and the bottom end of sorbent concentrations normally used for remediation via

adsorption. This work therefore extrapolates outside the conditions used to experimentally determine the model parameters, and the results should be considered as giving a semi-quantitative or qualitative comparison of batch and continuous-flow systems, based on identifying appropriate orders of magnitude in sorbent concentrations and flow-rates for treatment plant design.

3.4.1. Batch reactor design

Batch reactors treat a single volume of water until contaminant concentrations are within safety limits. The user waits for the water to be treated before collection, with longer treatments providing more complete removal of contaminants. Results from the batch treatment model are presented in Fig. 4, with kinetic profiles in Fig. 4a, and the time required to provide safe drinking water (< 10 µg L⁻¹) in Fig. 4b. The model predicted that 0.1 g L⁻¹ TiO₂-Fe₂O₃ could only successfully treat water contaminated with < 100 µg L⁻¹ As(III), and only with long treatment times on the hour timescale. At least 1 g L⁻¹ TiO₂-Fe₂O₃ was needed to treat As(III) contaminated water within 1 h, and even then, several hours of treatment was needed when C_0 was greater than 400 µg L⁻¹. With ≥ 10 g L⁻¹ sorbent, water contaminated with up to 2000 µg L⁻¹ As(III) was rapidly remediated within a matter of minutes. Our model suggests that for batch treatments using multi-functional photocatalyst-sorbent materials, more than the typical 0.01–0.1 g L⁻¹ photocatalyst loading is required for the sorbent to perform sufficiently. Furthermore, below 1 g L⁻¹ kinetic limitations are important, adding constraints on treatment time.

3.4.2. Continuous-flow reactor design

In a continuous-flow system, contaminated influent is continuously pumped into the reactor whilst treated effluent is extracted. Breakthrough curves for the continuous-flow model are given in Fig. 5(a) and (b). At high sorbent concentrations (≥ 100 g L⁻¹), varying the turnover rate between 0.001 and 0.1 min⁻¹ had little effect on the shape of the simulated breakthrough curve: the sorbent removed As(III) sufficiently fast that no build-up of aqueous As(III) in the reactor occurred prior to sorbent saturation. For more dilute TiO₂-Fe₂O₃ suspensions (≤ 10 g L⁻¹), however, the shape of the breakthrough curve in our model was strongly influenced by the turnover rate.

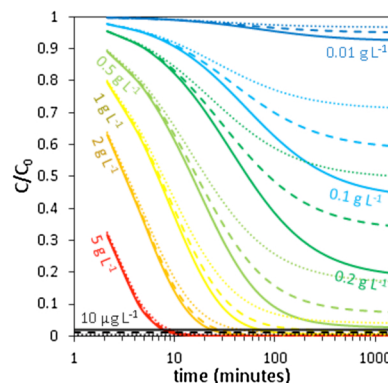
For instance, modelling suspensions of 10 g L⁻¹ sorbent under a slow turnover rate of 0.001 min⁻¹, breakthrough only occurred once the sorbent was saturated. With 500 µg L⁻¹ influent As(III), this corresponds to breakthrough above the WHO limit of 10 µg L⁻¹ after 14 bed volumes (Fig. 5c). When turnover frequency was increased to 0.01 min⁻¹, fewer bed volumes were treated before breakthrough due to kinetic limitations: breakthrough was reached after just 6 bed volumes. Formation of a steady state before breakthrough was also observed, with 4.5 µg L⁻¹ As(III) in the reactor. When turnover frequency was increased to 0.1 min⁻¹, breakthrough was reached after just 2.6 bed volumes. Here, the model predicted a steady state scenario with approximately 43 µg L⁻¹ As(III), already exceeding the WHO limit. Since breakthrough occurred with an unsaturated sorbent, due to the As(III) steady-state, this scenario represents an inefficient and

Table 3

Parameters used for kinetic adsorption modelling. The rate constant k' was determined from adsorption kinetics. Freundlich isotherm parameters were determined from adsorption isotherms, with K_F rescaled to account for the difference in q_e obtained between adsorption isotherms and adsorption kinetics. Errors indicate the 68% confidence interval.

Parameter	Label and units	Value
Rate constant	$k' (\text{L g}^{-1} \text{ min}^{-1})$	0.111 ± 0.015
Initial sorbate concentration	$C_0 (\mu\text{g L}^{-1})$	10–2000 (batch), 0 (continuous flow)
Initial sorbent concentration	$C_s (\text{g L}^{-1})$	0.01–10 000
Influent concentration	$C_{\text{influent}} (\mu\text{g L}^{-1})$	0 (batch), 500, 1000 and 2000 (continuous flow)
Turnover rate	$j (\text{min}^{-1})$	0 (batch), 0.001–1 (continuous flow)
Adsorption capacity (Freundlich parameters)	$K_F (\text{mg g}^{-1} (\text{mg L}^{-1})^{-1/n})$	5.10 ± 1.60
	$n (\text{unitless})$	2.63 ± 0.14

(a)



(b)

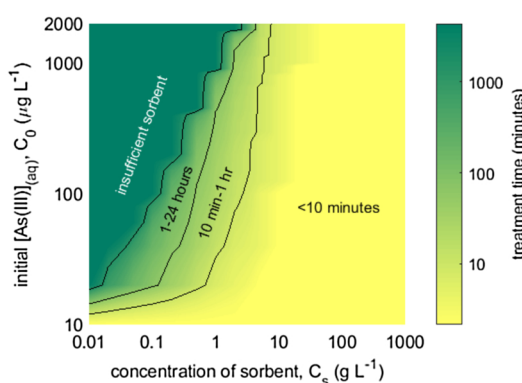


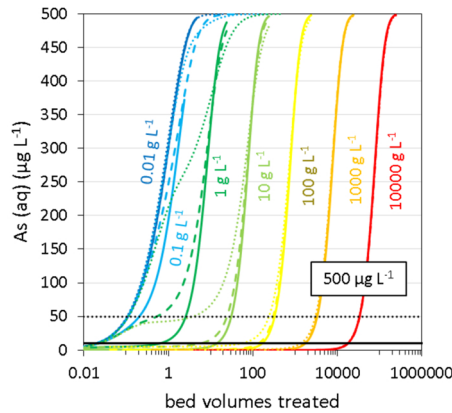
Fig. 4. Modelling batch treatment. (a) Batch kinetics predicted for As(III) adsorption using different concentrations of $\text{TiO}_2\text{-Fe}_2\text{O}_3$. The simulated kinetics are shown for initial As(III) concentrations of $500 \mu\text{g L}^{-1}$ (solid lines), $1000 \mu\text{g L}^{-1}$ (dashed lines) and $2000 \mu\text{g L}^{-1}$ (dotted lines). The black lines close to the x -axis indicate the $10 \mu\text{g L}^{-1}$ WHO arsenic guideline limit. (b) The time taken to remove arsenic below the $10 \mu\text{g L}^{-1}$ WHO limit, as a function of both initial As(III) concentration and sorbent loading. C_s refers to sorbent concentration and $[\text{As(III)}]_0$ is the initial concentration of aqueous As(III), C_0 .

uneconomical use of sorbent. Similar results were observed with $2000 \mu\text{g L}^{-1}$ (Fig. 5d), however the higher influent concentration leads to As(III) steady-states surpassing the guideline limits at lower turnover rates.

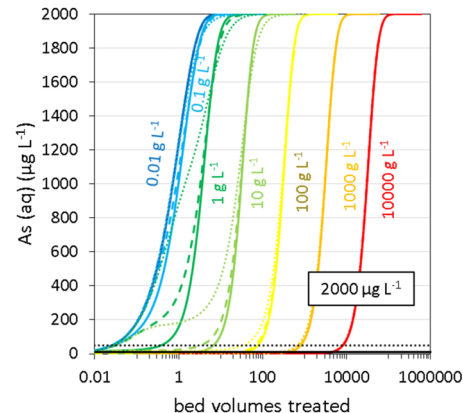
The results predicted by our model match experimental observations in similar systems: breakthrough at under-saturated conditions due to high flow-rates in the adsorption of As(V) onto laterite [52], and

steady-state breakthrough during As(V) adsorption onto both two-line ferrihydrite (an iron oxide) [53], and anion exchange beads [54]. Ideally, the sorbent is saturated at breakthrough: this is a more economical use of material, with the sorbent requiring replacement less often. The simulated results suggested that aiming to achieve a sorbent efficiency of at least 50%, with $< 10 \mu\text{g L}^{-1}$ As(III) in the effluent, and a turnover rate of $0.01 - 0.1 \text{ min}^{-1}$ (i.e. between 10 and 100 min treatment time),

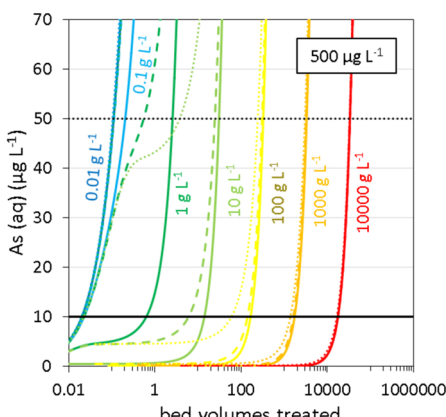
(a)



(b)



(c)



(d)

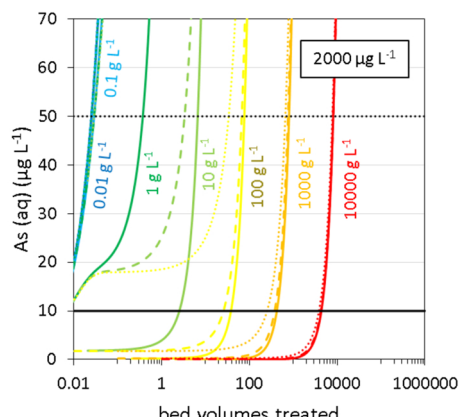
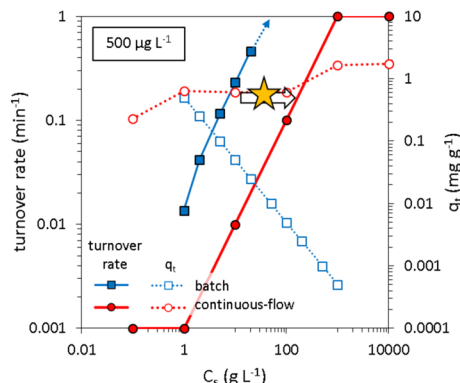
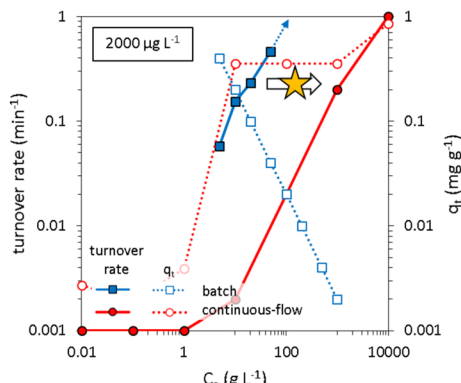


Fig. 5. Modelling continuous-flow treatment. Simulated As(III) breakthrough curves as a function of sorbent loading are presented with influent concentrations of (a) $500 \mu\text{g L}^{-1}$ and (b) $2000 \mu\text{g L}^{-1}$ As(III). (c) and (d) provide close ups of arsenic breakthrough and the formation of steady-states. Breakthrough curves were simulated at turnover rates of 0.001 (solid lines), 0.01 (dashed lines) and 0.1 (dotted lines) min^{-1} . Both the WHO $10 \mu\text{g L}^{-1}$ guideline limit (solid black lines) and the higher $50 \mu\text{g L}^{-1}$ limit (dashed black lines) are indicated.

(a)



(b)



sorbent efficiencies) between continuous-flow and batch treatment systems. (For interpretation of the references to the web version of this article.)

sorbent concentrations in the order of 100 g L^{-1} are needed to treat $500 \mu\text{g L}^{-1}$ influent As(III), and 1000 g L^{-1} sorbent is needed to treat $2000 \mu\text{g L}^{-1}$ influent As(III).

3.4.3. Comparison of reactor designs

A comparison between simulated results using the batch and continuous-flow treatment models is given in Fig. 6, showing both turnover rate (the reciprocal of treatment time, on the left-hand y-axis) and sorbent efficiency (as the quantity of sorbate adsorbed after successful treatment, or at breakthrough, on the right-hand y-axis) as a function of sorbent loading. For the continuous-flow system, the reported data was selected to give the best combination of turnover rate and sorbent efficiency (calculated as the product between the two).

For the batch treatment, the model gave a linear relationship between increasing C_s and turnover rate, as expected since the rate of As(III) removal in the model is first order with respect to C_s . The sorbent efficiency linearly decreased with increasing C_s , as the same quantity of arsenic in the reactor becomes distributed across an increasingly large sorbent mass.

The continuous-flow system also showed a linear increase between C_s and turnover rate, again due to the first order dependence of adsorption rate upon C_t within the model. However, unlike the batch system, the sorbent efficiency of continuous-flow treatment increased with increasing C_s . This was because at low values of C_s , breakthrough occurred with undersaturated sorbent, due to slow adsorption kinetics. At high values of C_s , kinetic limitations become less significant and the sorbent reached a higher degree of saturation before breakthrough.

As indicated by the stars in Fig. 6, the continuous-flow system was predicted to require between one and two orders of magnitude more sorbent (g L^{-1}) than the batch system to achieve the same sorbent efficiency (mg g^{-1}) at similar turnover rates (min^{-1}). For example, in the batch treatment, 10 g L^{-1} sorbent was sufficient to treat water contaminated with up to $2000 \mu\text{g L}^{-1}$ As(III) in less than 10 min (i.e. a turnover rate of 0.1 min^{-1}), whereas in the continuous flow model 1000 g L^{-1} was needed. This is logical, since in the batch treatment the entire quantity of sorbate is introduced to the sorbent at once, leading to much faster early adsorption kinetics (due to the first order dependency on C_t). The continuous-flow scenario is different, as the concentration of aqueous As(III) at each point in time (C_t) can never exceed $10 \mu\text{g L}^{-1}$ As(III) without breakthrough having been reached. The difference between batch and continuous-flow systems is more pronounced at higher sorbate concentrations, as the difference in C_t at $t = 0$ between batch and continuous-flow systems becomes more significant. The implication is that batch treatment may be more appropriate for scenarios requiring low sorbent concentrations (such as when using photocatalysis) and requiring a very large reduction in the

Fig. 6. Comparison of simulated results for batch (blue squares) and continuous-flow (red circles) treatments. Turnover rate (filled shapes and solid lines) and sorbent efficiency (open shapes, dotted lines) are given as a function of sorbent loading. For the continuous-flow system, a two-dimensional matrix of experiments, varying in C_s and turnover rate, was simulated. To reduce the two independent variables to just one (C_s), the data shown corresponds to the ‘optimum’ turnover rate identified at each value of C_s , determined as the value of turnover rate giving the highest product of j and q_b , i.e. an equal priority weighting for turnover rate and sorbent efficiency. The arrow labelled with a star denotes the shift in sorbent concentration required to achieve similar performance (turnover and

relative concentration of contaminants (e.g. reducing $2000 \mu\text{g L}^{-1}$ As(III) to just $10 \mu\text{g L}^{-1}$). These results suggest that for a one-off remediation, batch treatment is more appropriate than continuous-flow, with faster treatment times and the same sorbent efficiencies, but only if the appropriate mass of sorbent can be identified to minimise surplus sorbent and thus achieve good sorbent economies.

3.5. Modelling a 365-day deployment

3.5.1. Daily household water requirements and boundary conditions

As discussed, historic failings of South Asia mitigation schemes designed around sorbent filters include the difficulty users find when cleaning saturated media [16], carrying out maintenance, and the limited market availability of fresh sorbent media to replace saturated media [24,17]. We therefore wanted to explore how batch and continuous-flow treatments would compare if the sorbent was used for an entire year before replenishment. The best solution would provide safe, potable water ($< 10 \mu\text{g L}^{-1}$ arsenic) for 365 days, using the least sorbent, due to the need for cost efficiency [16].

As boundary conditions for the volume of potable water required, we considered the needs of a rural family in West Bengal, India, with an average of 5.7 people per household [55]. The WHO South-East Asia Technical Office reports that 7 L of water is required per person per day (4 L per capita per day (Lpcd) for drinking and 3 Lpcd for food preparation) [56]. These two figures give a requirement of 40 L day^{-1} potable water per household. This is equivalent to $14,600 \text{ L per year}$ per household, and where $C_0 = 500 \mu\text{g L}^{-1}$ As(III), equates to the removal of 7.3 g of arsenic per year. Flow rate was not considered an essential parameter, as whilst the WHO specifies that the flow rate at each collection point should be at least $0.125 \text{ L per second}$ [56], in cases where treatment is slow, effluent can be collected in a storage tank prior to distribution, as is the case in current treatment plants [20].

3.5.2. Modelling sequential batch treatments

To model a 365-day deployment, the continuous-flow MATLAB code was used without modification. For the batch treatment system, codes were modified to represent gradual saturation of the media during 365 sequential treatments. A selection of simulated results are presented in Fig. 7, highlighting the inverse relationship between initial sorbate concentration, C_0 , and the number of days successfully treated.

3.5.3. Comparison of batch and continuous-flow treatments

The 365-day models predicted that the batch treatment would provide safe water for at least as many days as the continuous-flow design under all combinations of C_s and treatment time (Table 4). For the batch reactor, the number of days per year with successful As(III)

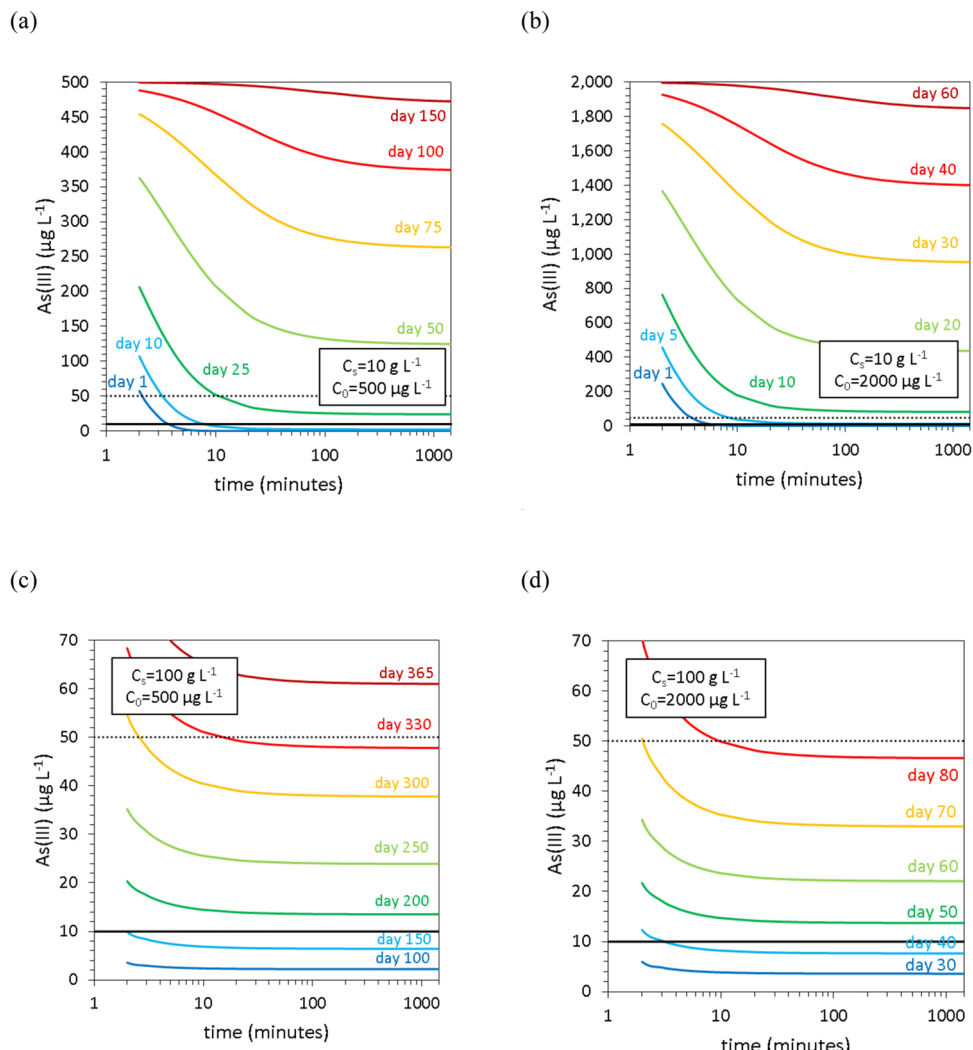


Fig. 7. Kinetic adsorption modelling: batch treatment using the same sorbent for 365 days. Shown are kinetic profiles for simulations using 10 g L^{-1} sorbent and initial As(III) concentrations of $500 \mu\text{g L}^{-1}$ (a), and $2000 \mu\text{g L}^{-1}$ (b), and 100 g L^{-1} sorbent with initial As(III) concentrations of (c) $500 \mu\text{g L}^{-1}$, and (d) $2000 \mu\text{g L}^{-1}$. For each simulation after day 1, the initial amount of adsorbed As(III) (q_t) was set as the final value of q_t for the simulation representing the previous day, reflecting the sorbent becoming saturated through repeat use. The WHO $10 \mu\text{g L}^{-1}$ guideline limit (solid black lines) and $50 \mu\text{g L}^{-1}$ limit (dashed black lines) are indicated.

removal depended primarily on sorbent loading and was not significantly affected by the treatment time: batch treatment was rapid due to the fast kinetics during initial mixing, resulting from the high

initial concentration of As(III) and first order dependence on C_r . However, for the continuous-flow reactor, sorbent loading and flow rate (turnover rate) were equally important; for instance, reducing the flow

Table 4

Comparison of results from modelling 365-day sorbent deployments in batch and continuous-flow configurations. The table presents the number of days during which water was successfully treated for (a) batch and (b) continuous-flow systems as a function of sorbent loading and the average residence time, with $500 \mu\text{g L}^{-1}$ initial As(III).

Batch treatment								Continuous-flow treatment							
Treatment time (min)	Sorbent concentration (g L^{-1})							Residence time (min)	Sorbent concentration (g L^{-1})						
	0.01	0.1	1	10	100	1000	10,000		0.01	0.1	1	10	100	1000	10,000
1	0	0	0	0	100	365	365	1	0	0	0	0	1	12	
2	0	0	0	0	150	365	365	2	0	0	0	0	0	1	21
5	0	0	0	5	150	365	365	5	0	0	0	0	0	4	56
10	0	0	0	10	150	365	365	10	0	0	0	0	0	10	115
20	0	0	0	15	175	365	365	20	0	0	0	0	1	21	236
50	0	0	0	15	175	365	365	50	0	0	0	0	4	56	365
100	0	0	1	17	175	365	365	100	0	0	0	0	10	115	365
200	0	0	1	17	175	365	365	200	0	0	0	1	21	236	365
500	0	0	1	17	175	365	365	500	0	0	0	4	56	365	365
1000	0	0	1	17	178	365	365	1000	0	0	0	10	115	365	365

rate by a factor of 10 had the same effect on the number of days with successful treatment as multiplying the sorbent concentration by a factor of 10. This was due to high turnover rates (short residence times) leading to As(III) breakthrough before the sorbent was saturated: the concentration of As(III) in the continuous-flow reactor was always $< 10 \mu\text{g L}^{-1}$ before breakthrough, and adsorption kinetics were therefore limited by the first order dependence on C_s .

The model suggested that the batch reactor would prove more successful when treatment times are shortened. For instance, in the batch model, 100 g L^{-1} sorbent successfully removed $500 \mu\text{g L}^{-1}$ As(III) for 175 days with a treatment time of just 20 min per day (Table 4). In contrast, 100 g L^{-1} sorbent in the continuous-flow system failed to treat water contaminated with $500 \mu\text{g L}^{-1}$ As(III) with 20 min average residence time after just one day (Table 4). The implication is that batch reactor designs may be more economical: shorter treatment times in a batch reactor mean that energy intensive processes such as pumping, mixing and ultraviolet irradiation might be performed for shorter durations.

3.5.4. Economising sorbent use

A minimum sorbent concentration of 1 kg L^{-1} was required to safely remove As(III) for an entire year in both reactor designs. This is much higher than typical photocatalyst concentrations. Whilst treatments in the hours timescale were needed for continuous-flow, batch treatment was successful in just minutes. However, the best sorbent economies were achieved under conditions wherein the sorbent needed replacing during the 365-day deployment (Fig. 8). At the slowest treatment times (1000 minutes, approximating a reactor operated continuously all day), batch treatments gave the best sorbent economy when sorbent concentration was less than 100 g L^{-1} , whilst continuous-flow treatments gave a better sorbent economy with $C_s > 100 \text{ g L}^{-1}$ (Fig. 8). Further results on sorbent economy are given in the Supplementary Information.

The minimum mass of sorbent required was similar between batch and continuous-flow models, with 8.2 and 8.4 kg sorbent household $^{-1}$ year $^{-1}$ respectively (when initial As(III) concentrations were $500 \mu\text{g L}^{-1}$). However, the conditions under which optimal sorbent economies were obtained varied between the two systems. Sorbent economy was best in the batch model when using 100 g L^{-1} sorbent and treatment times of 1000 min (8.2 kg sorbent household $^{-1}$ year $^{-1}$), however similar results were achieved with less sorbent and faster treatment times: 10 g L^{-1} sorbent and 100 min treatment times gave a sorbent requirement of 8.6 kg household $^{-1}$ year $^{-1}$. When $C_s = 10 \text{ g L}^{-1}$ and 100 g L^{-1} , the sorbent required replacing every 17 and 175 days, respectively. In the continuous-flow model, the best sorbent economy was achieved with much higher sorbent concentrations: $C_s = 1$ and 10 kg L^{-1} , and treatment times of 200 and 20 min

respectively. Under these conditions, 8.6 kg sorbent household $^{-1}$ year $^{-1}$ was required and the sorbent would require replacing every 236 days. The batch model therefore provided better sorbent economies at low sorbent concentrations, again suggesting that this is the more appropriate reactor design for photocatalyst-sorbent systems.

The $\sim 8 \text{ kg}$ of sorbent per household per year is only an estimation, as a number of factors will affect the true amount of sorbent needed. For instance, As(III) has been considered in the absence of competitor ions which suppress adsorption. Secondly, multilayer surface precipitation effects are important for both As(III) and As(V), increasing arsenic removal [46,57]. Surface precipitation is a much slower process than adsorption and is thus unlikely to have been captured in our experimental determination of As(III) adsorption kinetics.

3.6. Implications for engineering photocatalyst-sorbent systems

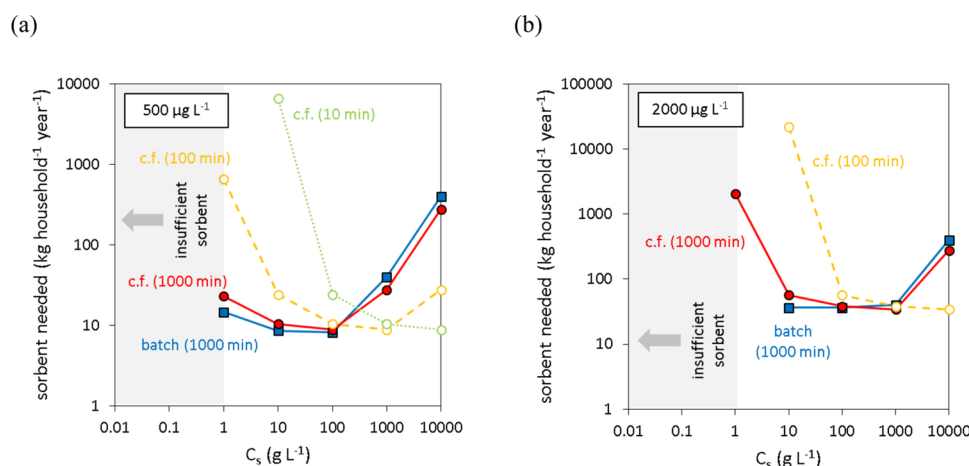
The simulated models suggested that batch treatments are more efficient than continuous-flow when the sorbent concentration is limited (i.e. $< 10 \text{ g L}^{-1}$), for both single use and long-term deployment. Since most applications of photocatalysts for water remediation use low catalyst concentrations, the batch reactor design appears most promising for the application of multifunctional composite-sorbents such as $\text{TiO}_2-\text{Fe}_2\text{O}_3$. The model also suggested that more than 100 g L^{-1} is required for a year's treatment without changing media: this is much greater than typical photocatalyst concentrations. Consequently, to operate at 1 g L^{-1} and under, the $\text{TiO}_2-\text{Fe}_2\text{O}_3$ media would need to be replenished several times per year.

The batch reactor design is 'safer' in the sense that there is less dependency on treatment time due to the fast removal in the initial minutes of treatment thanks to high C_s , with sorbent loading being the principal parameter. By using excess concentrations of sorbent, water can be treated rapidly without breakthrough. Our results contrast with Lekić et al. who observed experimentally that As(III) and As(V) removal per gram of sorbent was superior in a column (continuous-flow) configuration compared with batch treatment, which they posited as being due to non-adsorption processes such as coagulation, flocculation and filtration, that were not included in our present model [23]. Our recommendation is thus that photooxidation kinetics in the photocatalyst-sorbent system be studied at high material concentrations ($\geq 10 \text{ g L}^{-1}$), and with different reactor dimensions, to verify that suspensions can be sufficiently irradiated to provide effective photooxidation at the high sorbent concentrations needed to achieve sufficient device lifetimes.

4. Conclusions

This work aimed to address the question of how much sorbent is needed in a reactor for As(III) remediation based on $\text{TiO}_2-\text{Fe}_2\text{O}_3$

Fig. 8. Comparison of results from modelling 365-day sorbent deployments in batch and continuous-flow configurations. Sorbent efficiency (kg sorbent required per household per year) is presented as a function of sorbent concentration, and with different treatment times, where initial As(III) concentrations are (a) $500 \mu\text{g L}^{-1}$ and (b) $2000 \mu\text{g L}^{-1}$. Note that some data points correspond to scenarios wherein the sorbent has failed to provide 365 days of safe water. Continuous-flow is abbreviated as 'c.f.', the batch model is given as blue squares, and continuous-flow as (i) red circles-solid lines (1000 min average residence time), (ii) open circles-yellow dashed lines (100 min), and (iii) open circles-green dotted lines (10 min). (For interpretation of the references to color in this figure legend, the reader is referred to the web version of this article.)



composite photocatalyst-sorbent technology. We considered the conservative scenario that the material is acting as a sorbent only. Our findings are:

- (a) Material concentrations significantly greater than the $0.01 - 0.1 \text{ g L}^{-1}$ photocatalyst concentrations normally used in the literature are needed for $\text{TiO}_2\text{-Fe}_2\text{O}_3$ to effectively remove As(III) from contaminated waters through adsorption;
- (b) Kinetic modelling predicts that batch treatment processes are preferred over continuous flow for the adsorption of As(III) at sorbent concentrations below 100 g L^{-1} . Batch processes should be considered in preference to continuous-flow, given that sorbent concentrations should be minimised to provide sufficient penetration of light through suspension;
- (c) With 10 g L^{-1} $\text{TiO}_2\text{-Fe}_2\text{O}_3$ or less, the media would need to be replenished multiple times throughout the year to maintain effective treatment;
- (d) Continuous flow only offers more economical use of sorbent at high sorbent concentrations ($> 100 \text{ g L}^{-1}$).

On the basis of this study, we recommend subsequent experimental work on multifunctional photocatalyst-sorbent materials to consider the influence of material concentration on photooxidation kinetics, given that concentrations above 10 g L^{-1} may be required for effective adsorption of contaminants such as arsenic. An experimental comparison of batch and continuous-flow reactors using photocatalyst-sorbent technology is required. This kinetic adsorption model may be further advanced through introduction of experimental photooxidation rates to provide further insights into how photocatalyst-sorbent materials might be applied in engineered applications towards the remediation of As(III) contaminated waters.

CRediT authorship contribution statement

Jay C. Bullen: Conceptualization, Methodology, Software, Validation, Formal analysis, Investigation, Writing - original draft, Writing - review & editing, Visualization. **Chaipat Lapinee:** Formal analysis, Investigation, Writing - review & editing, Visualization. **Pascal Salaün:** Methodology, Resources, Writing - review & editing. **Ramon Vilar:** Resources, Writing - review & editing, Supervision, Project administration, Funding acquisition. **Dominik J. Weiss:** Conceptualization, Resources, Writing - review & editing, Supervision, Project administration, Funding acquisition.

Declaration of Competing Interest

The authors declare that they have no known competing financial interests or personal relationships that could have appeared to influence the work reported in this paper.

Acknowledgements

The authors acknowledge support from the Engineering Physical Sciences Research Council (EPSRC) (Grant number EP/N509486/1), the William J Kenan Charitable Trust, the Royal Thai Government and from the University of Phayao. The authors also thank Dr Jens Narkoja from the Natural History Museum, UK, for providing XRD analysis.

Appendix A. Supplementary data

Supplementary material related to this article can be found, in the online version, at doi:<https://doi.org/10.1016/j.jece.2020.104033>.

References

- [1] A. Kumar, M. Biswas, P.K. Roy, J.M. Wallace, Assessment of arsenic removal units in Arsenic-Prone Rural Area in Uttar Pradesh, India, *J. Inst. Eng. Ser. A* (2019), <https://doi.org/10.1007/s40030-018-0349-9>.
- [2] J.G. Hering, I.A. Katsiyannis, G.A. Theoduloz, M. Berg, S.J. Hug, Arsenic removal from drinking water: experiences with technologies and constraints in practice, *J. Environ. Eng. (United States)* 143 (2017) 1–9, [https://doi.org/10.1061/\(ASCE\)EE.1943-7870.0001225](https://doi.org/10.1061/(ASCE)EE.1943-7870.0001225).
- [3] S. Sorlini, F. Gialdini, Conventional oxidation treatments for the removal of arsenic with chlorine dioxide, hypochlorite, potassium permanganate and monochloramine, *Water Res.* 44 (2010) 5653–5659, <https://doi.org/10.1016/j.watres.2010.06.032>.
- [4] V.K. Sharma, M. Sohn, Aquatic arsenic: toxicity, speciation, transformations, and remediation, *Environ. Int.* 35 (2009) 743–759, <https://doi.org/10.1016/j.envint.2009.01.005>.
- [5] E.E. Lavonen, M. Gonsior, L.J. Tranvik, P. Schmitt-Kopplin, S.J. Köhler, Selective chlorination of natural organic matter: identification of previously unknown disinfection byproducts, *Environ. Sci. Technol.* 47 (2013) 2264–2271, <https://doi.org/10.1021/es304669p>.
- [6] Z. Zhang, J. Gamage, Applications of photocatalytic disinfection, *Int. J. Photoenergy.* 2010 (2010), <https://doi.org/10.1155/2010/764870>.
- [7] W. Zhou, H. Fu, K. Pan, C. Tian, Y. Qu, P. Lu, C. Sun, Mesoporous $\text{TiO}_2\text{/}\alpha\text{-Fe}_2\text{O}_3$: multifunctional composites for effective elimination of arsenite contamination through simultaneous photocatalytic oxidation and adsorption, *J. Phys. Chem.* 112 (2008) 19584–19589, <https://doi.org/10.1021/jp806594m>.
- [8] L. Yu, X. Peng, F. Ni, J. Li, D. Wang, Z. Luan, Arsenite removal from aqueous solutions by $\gamma\text{-Fe}_2\text{O}_3\text{-TiO}_2$ magnetic nanoparticles through simultaneous photocatalytic oxidation and adsorption, *J. Hazard. Mater.* 246–247 (2013) 10–17, <https://doi.org/10.1016/j.jhazmat.2012.12.007>.
- [9] H. Su, X. Lv, Z. Zhang, J. Yu, T. Wang, Arsenic removal from water by photocatalytic functional $\text{Fe}_2\text{O}_3\text{-TiO}_2$ porous ceramic, *J. Porous Mater.* 24 (2017) 1227–1235, <https://doi.org/10.1007/s10934-017-0362-9>.
- [10] R.I. Bickley, M.J. Slater, W.J. Wang, Engineering development of a photocatalytic reactor for waste water treatment, *Process Saf. Environ. Prot.* 83 (2005) 205–216, <https://doi.org/10.1205/psep.04028>.
- [11] A. Yerkinova, G. Balbayeva, V.J. Inglezakis, S.G. Poulopoulos, Photocatalytic treatment of a synthetic wastewater, *IOP Conf. Ser. Mater. Sci. Eng.* 301 (2018), <https://doi.org/10.1088/1757-899X/301/1/012143>.
- [12] C. Ferreiro, N. Villota, J.I. Lombrana, M.J. Rivero, V. Zúñiga, J.M. Rituerto, Analysis of a hybrid suspended-supported photocatalytic reactor for the treatment of wastewater containing benzothiazole and aniline, *Water (Switzerland)* 11 (2019), <https://doi.org/10.3390/w11020337>.
- [13] P.K. Dutta, S.O. Pehkonen, V.K. Sharma, A.K. Ray, Photocatalytic oxidation of arsenic(III): evidence of hydroxyl radicals, *Environ. Sci. Technol.* 39 (2005) 1827–1834, <https://doi.org/10.1021/es0489238>.
- [14] V. Vaiano, G. Iervolino, D. Sannino, L. Rizzo, G. Sarno, A. Farina, Enhanced photocatalytic oxidation of arsenite to arsenate in water solutions by a new catalyst based on MoO_x supported on TiO₂, *Appl. Catal. B Environ.* 160–161 (2014) 247–253, <https://doi.org/10.1016/j.apcatb.2014.05.034>.
- [15] E. Colombo, M. Ashokkumar, Comparison of the photocatalytic efficiencies of continuous stirred tank reactor (CSTR) and batch systems using a dispersed micron sized photocatalyst, *RSC Adv.* 7 (2017) 48222–48229, <https://doi.org/10.1039/c7ra09753k>.
- [16] R.B. Johnston, S. Hanchett, M.H. Khan, The socio-economics of arsenic removal, *Nat. Geosci.* 3 (2010) 2–3, <https://doi.org/10.1038/ngeo735>.
- [17] M. Shafiquzzaman, M.S. Azam, I. Moshima, J. Nakajima, Technical and Social evaluation of arsenic mitigation in rural Bangladesh, *J. Heal. Popul. Nutr.* 27 (2009) 674–683, <https://doi.org/10.3329/jhpn.v27i5.3779>.
- [18] M.S. German, T.A. Watkins, M. Chowdhury, P. Chatterjee, M. Rahman, Evidence of economically sustainable village-scale microenterprises for arsenic remediation in developing countries, *Env. Sci. Technol.* (2019), <https://doi.org/10.1021/acs.est.8b02523>.
- [19] A.B. Dichiara, S.J. Weinstein, R.E. Rogers, On the choice of batch or fixed bed adsorption processes for wastewater treatment, *Ind. Eng. Chem. Res.* 54 (2015) 8579–8586, <https://doi.org/10.1021/acs.iecr.5b02350>.
- [20] A. Bhardwaj, R. Rajput, K. Misra, Status of Arsenic Remediation in India, Elsevier Inc., 2019, <https://doi.org/10.1016/b978-0-12-814790-0-00009-0>.
- [21] C. McCullagh, N. Skillen, M. Adams, P.K.J.J. Robertson, Photocatalytic reactors for environmental remediation: a review, *J. Chem. Technol. Biotechnol.* 86 (2011) 1002–1017, <https://doi.org/10.1002/jctb.2650>.
- [22] I. Ali, Z.A. Al-Othman, A. Alwarthan, M. Asim, T.A. Khan, Removal of arsenic species from water by batch and column operations on bagasse fly ash, *Environ. Sci. Pollut. Res.* 21 (2014) 3218–3229, <https://doi.org/10.1007/s11356-013-2235-3>.
- [23] B.M. Lekić, D.D. Marković, V.N. Rajaković-Ognjanović, A.R. Dukić, L.V. Rajaković, Arsenic removal from water using industrial by-products, *J. Chem.* 2013 (2013), <https://doi.org/10.1155/2013/121024>.
- [24] D.K. Kundu, A.P.J. Mola, A. Gupta, Failing arsenic mitigation technology in rural Bangladesh: explaining stagnation in niche formation of the Sono filter, *Water Policy* 18 (2016) 1490–1507, <https://doi.org/10.2166/wp.2016.014>.
- [25] The Failing Response to Arsenic in the Drinking Water of Bangladesh's Rural Poor | HRW, (n.d.). <https://www.hrw.org/report/2016/04/06/nepotism-and-neglect/failing-response-arsenic-drinking-water-bangladesh-rural> (Accessed 15 June 2017).
- [26] S.R. Khandker, H.A. Samad, R. Ali, D.F. Barnes, Who benefits most from rural

- electrification? Evidence in India, *Energy J.* (2014), <https://doi.org/10.5547/01956574.35.2.4>.
- [27] M. D'Arcy, D. Weiss, M. Bluck, R. Vilar, Adsorption kinetics, capacity and mechanism of arsenate and phosphate on a multifunctional $\text{TiO}_2\text{-Fe}_2\text{O}_3$ bi-composite, *J. Colloid Interface Sci.* 364 (2011) 205–212, <https://doi.org/10.1016/j.jcis.2011.08.023>.
- [28] K. Liu, H. Fu, K. Shi, F. Xiao, L. Jing, B. Xin, Preparation of large-pore mesoporous nanocrystalline TiO_2 thin films with tailored pore diameters, *J. Phys. Chem. B* 109 (2005) 18719–18722, <https://doi.org/10.1021/jp054546p>.
- [29] N. Ayawei, A.N. Ebelegi, D. Wankasi, Modelling and interpretation of adsorption isotherms, *J. Chem.* 2017 (2017), <https://doi.org/10.1155/2017/3039817>.
- [30] Y.S. Ho, G. McKay, Pseudo-second order model for sorption processes, *Process Biochem.* 34 (1999) 451–465, [https://doi.org/10.1016/S0032-9592\(98\)00112-5](https://doi.org/10.1016/S0032-9592(98)00112-5).
- [31] K. Gibbon-Walsh, P. Salaün, M.K. Uroic, J. Feldmann, J.M. McArthur, C.M.G. Van Den Berg, Voltammetric determination of arsenic in high iron and manganese groundwaters, *Talanta* 85 (2011) 1404–1411, <https://doi.org/10.1016/j.talanta.2011.06.038>.
- [32] A. Cheng, R. Tyne, Y.T. Kwok, L. Rees, L. Craig, C. Lapinee, M. D'Arcy, D.J. Weiss, P. Salaün, Investigating arsenic contents in surface and drinking water by Voltammetry and the method of standard additions, *J. Chem. Educ.* (2016), <https://doi.org/10.1021/acs.jchemed.6b00025>.
- [33] J.C. Bullen, A. Torres-huerta, P. Salaün, J.S. Watson, S. Majumdar, R. Vilar, D.J. Weiss, Portable and rapid arsenic speciation in synthetic and natural waters by an As(V)-selective chemisorbent, validated against anodic stripping voltammetry, *Water Res.* 175 (2020) 115650, , <https://doi.org/10.1016/j.watres.2020.115650>.
- [34] W. Hu, J. Xie, H.W. Chau, B.C. Si, Evaluation of parameter uncertainties in non-linear regression using Microsoft Excel Spreadsheet, *Environ. Syst. Res.* 4 (2015), <https://doi.org/10.1186/s40068-015-0031-4>.
- [35] J.C. Bullen, S. Saleesongsom, D.J. Weiss, A revised pseudo-second order kinetic model for adsorption, sensitive to changes in sorbate and sorbent concentrations, *ChemRxiv Prepr.* (2020), <https://doi.org/10.26434/chemrxiv.12008799>.
- [36] A.W. Marczewski, Analysis of kinetic langmuir model. Part I: integrated kinetic langmuir equation (IKL): a new complete analytical solution of the langmuir rate equation, *Langmuir* 26 (2010) 15229–15238, <https://doi.org/10.1021/la1010049>.
- [37] Y. Huang, M.U. Farooq, S. Lai, X. Feng, P. Sampranpiboon, X. Wang, W. Huang, Model fitting of sorption kinetics data: misapplications overlooked and their rectifications, *AIChE J.* 64 (2018) 1793–1805, <https://doi.org/10.1002/aic.16051>.
- [38] J.C. Bullen, MATLAB Codes - a Kinetic Adsorption Model for Modelling Arsenic Treatment Plant (ATP) Lifetimes, (2020), <https://doi.org/10.5281/zenodo.3690170>.
- [39] D. Chakraborti, M.M. Rahman, A. Mukherjee, M. Alauddin, M. Hassan, R.N. Dutta, S. Pati, S.C. Mukherjee, S. Roy, Q. Quamruzzman, M. Rahman, S. Morshed, T. Islam, S. Sorif, M. Selim, M.R. Islam, M.M. Hossain, Groundwater arsenic contamination in Bangladesh-21 Years of research, *J. Trace Elem. Med. Biol.* 31 (2015) 237–248, <https://doi.org/10.1016/j.jtemb.2015.01.003>.
- [40] K.K. Gupta, N.L. Singh, A. Pandey, S.K. Shukla, S.N. Upadayay, V. Mishra, P. Srivastava, N.P. Lalla, P.K. Mishra, Effect of Anatase/Rutile TiO_2 phase composition on arsenic adsorption, *J. Dispers. Sci. Technol.* 34 (2013) 1043–1052, <https://doi.org/10.1080/01932691.2012.735937>.
- [41] W. Tang, Q. Li, S. Gao, J.K. Shang, Arsenic (III,V) removal from aqueous solution by ultrafine $\alpha\text{-Fe}_2\text{O}_3$ nanoparticles synthesized from solvent thermal method, *J. Hazard. Mater.* 192 (2011) 131–138, <https://doi.org/10.1016/j.jhazmat.2011.04.111>.
- [42] Z. Wei, K. Liang, Y. Wu, Y. Zou, J. Zuo, D.C. Arriagada, Z. Pan, G. Hu, The effect of pH on the adsorption of arsenic(III) and arsenic(V) at the TiO_2 anatase [101] surface, *J. Colloid Interface Sci.* 462 (2016) 252–259, <https://doi.org/10.1016/j.jcis.2015.10.018>.
- [43] J. Giménez, M. Martínez, J. de Pablo, M. Rovira, L. Duro, Arsenic sorption onto natural hematite, magnetite, and goethite, *J. Hazard. Mater.* 141 (2007) 575–580, <https://doi.org/10.1016/j.jhazmat.2006.07.020>.
- [44] P.K. Dutta, A.K. Ray, V.K. Sharma, F.J. Millero, Adsorption of arsenate and arsenite on titanium dioxide suspensions, *J. Colloid Interface Sci.* 278 (2004) 270–275, <https://doi.org/10.1016/j.jcis.2004.06.015>.
- [45] N. Deedar, A. Irfan, Q.I. A, Evaluation of the adsorption potential of titanium dioxide nanoparticle for arsenic removal, *J. Environ. Sci. China (China)* 21 (2009) 402–408, [https://doi.org/10.1016/S1001-0742\(08\)62283-4](https://doi.org/10.1016/S1001-0742(08)62283-4).
- [46] G. Morin, Y. Wang, G. Ona-Nguema, F. Juillet, G. Calas, N. Menguy, E. Aubry, J.R. Bargar, G.E. Brown, EXAFS and HRTEM evidence for As(III)-containing surface precipitates on nanocrystalline magnetite: Implications for arsenic sequestration, *Langmuir* 25 (2009) 9119–9128, <https://doi.org/10.1021/la900655v>.
- [47] C. Feng, C. Aldrich, J.J. Eksteen, D.W.M. Arrigan, Removal of arsenic from alkaline process waters of gold cyanidation by use of $\gamma\text{-Fe}_2\text{O}_3@\text{ZrO}_2$ nanosorbents, *Hydrometallurgy* 174 (2017) 71–77, <https://doi.org/10.1016/j.hydromet.2017.09.007>.
- [48] M. Pena, X. Meng, C. Jing, G. Korfiatis, C. Jing, Adsorption Mechanism of Arsenic on Nanocrystalline Titanium Dioxide, (2006), pp. 1257–1262, <https://doi.org/10.1021/es052040e>.
- [49] X. Yang, L. Xia, J. Li, M. Dai, G. Yang, S. Song, Adsorption of As(III) on porous hematite synthesized from goethite concentrate, *Chemosphere* 169 (2017) 188–193, <https://doi.org/10.1016/j.chemosphere.2016.11.061>.
- [50] R. Liu, J.F. Liu, L.Q. Zhang, J.F. Sun, G. Bin Jiang, Low temperature synthesized ultrathin $\gamma\text{-Fe}_2\text{O}_3$ nanosheets show similar adsorption behaviour for As(III) and As(v), *J. Mater. Chem. A Mater. Energy Sustain.* 4 (2016) 7606–7614, <https://doi.org/10.1039/c6ta01217e>.
- [51] Y. Li, N. Zhang, J. Chen, R. Li, L. Li, K. Li, Fabrication of $\alpha\text{-Fe}_2\text{O}_3/\text{TiO}_2$ bi-functional composites with hierarchical and hollow structures and their application in water treatment, *J. Nanopart. Res.* 18 (2016) 1–8, <https://doi.org/10.1007/s11051-016-3336-y>.
- [52] A. Maiti, S. DasGupta, J.K. Basu, S. De, Batch and column study: adsorption of arsenate using untreated laterite as adsorbent, *Ind. Eng. Chem. Res.* 47 (2008) 1620–1629, <https://doi.org/10.1021/ie070908z>.
- [53] H. Zeng, M. Arashiro, D.E. Giamarro, Effects of water chemistry and flow rate on arsenate removal by adsorption to an iron oxide-based sorbent, *Water Res.* 42 (2008) 4629–4636, <https://doi.org/10.1016/j.watres.2008.08.014>.
- [54] L. Dominguez, J. Economy, K. Benak, C.L. Mangun, Anion exchange fibers for arsenate removal derived from a vinylbenzyl chloride precursor, *Polym. Adv. Technol.* 14 (2003) 632–637, <https://doi.org/10.1002/pat.385>.
- [55] S. Sarkar, Consumption pattern and determinants of nutritional intake among rural households of West bengal, India, *J. Settlements Spat. Plan.* 6 (2015) 85–94.
- [56] WHO/SEARO, Minimum Water Quantity Needed for Domestic Uses, Technical Notes for Emergencies, 2005.
- [57] Y. Jia, L. Xu, Z. Fang, G.P. Demopoulos, Observation of surface precipitation of arsenate on ferrihydrite, *Environ. Sci. Technol.* 40 (2006) 3248–3253, <https://doi.org/10.1021/es051872+>.